

See discussions, stats, and author profiles for this publication at: <https://www.researchgate.net/publication/281102079>

High Strength Bimodal Amphiphilic Conetworks for Immunoisolation Membranes: Synthesis, Characterization, and Properties

ARTICLE *in* MACROMOLECULES · AUGUST 2015

Impact Factor: 5.8 · DOI: 10.1021/acs.macromol.5b01343

READS

28

6 AUTHORS, INCLUDING:



Gustavo Guzman

University of Akron

5 PUBLICATIONS 13 CITATIONS

[SEE PROFILE](#)



Joseph P Kennedy

University of Akron

579 PUBLICATIONS 7,956 CITATIONS

[SEE PROFILE](#)



Miko Cakmak

University of Akron

181 PUBLICATIONS 2,417 CITATIONS

[SEE PROFILE](#)

High Strength Bimodal Amphiphilic Conetworks for Immunoisolation Membranes: Synthesis, Characterization, and Properties

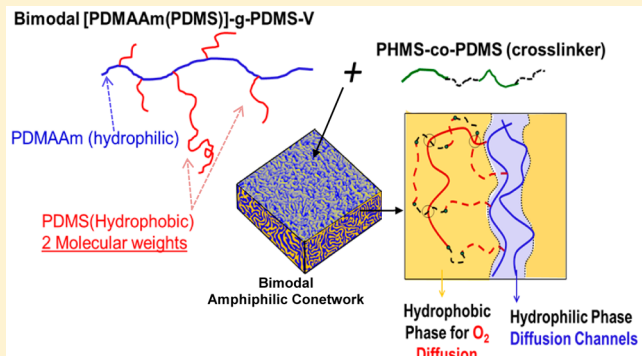
Gustavo Guzman,[†] Turgut Nugay,[§] Isil Nugay,[†] Nihan Nugay,[§] Joseph Kennedy,[‡] and Mukerrem Cakmak*,[†]

[†]Polymer Engineering Department and [‡]Polymer Science Department, The University of Akron, Akron, Ohio 44325, United States

[§]Chemistry Department, Polymer Research Center, Boğaziçi University, 34342 Bebek, Istanbul, Turkey

Supporting Information

ABSTRACT: A strategy for the synthesis of new cross-linkable bimodal amphiphilic grafts (bAPGs) was developed. These grafts are of hydrophilic PDMAAm backbones carrying low ($M_n \sim 17\,200$ g/mol) and high ($M_n \sim 117\,000$ g/mol) molecular weight hydrophobic PDMS branches, each branch carrying a vinylsilyl end-group. The bAPGs were cross-linked by Karstedt catalyst to bimodal amphiphilic conetworks (bAPCNs) by the use of polyhydrosiloxane-co-PDMS as the cross-linker. Membranes prepared from bAPCNs exhibit mechanical properties surprisingly superior to earlier APCNs prepared with APGs with monomodal low molecular weight branches. Membrane bimodality controls surface morphology and topography by means of elastic wrinkling instability during film formation. Semipermeable bAPCN membranes with precisely controlled nanochannel dimensions were prepared so as to allow rapid insulin diffusion and prevent passage of IgG. bAPCN membranes were designed for immunoprotection of live pancreatic islets and are thus key components for a bioartificial pancreas.



1. INTRODUCTION

A bioartificial pancreas is an implantable device which encapsulates and protects live pancreatic islets that release insulin and control blood sugar levels like a biological native pancreas. Among the critical issues in tissue encapsulation are evading foreign body response, avoiding unspecific protein adsorption (fouling) and biofilm formation, enabling oxygen penetration to the core of the device, filling the device without damaging islets, and placing the device close to the blood supply. Various strategies have been explored to extend the life and efficacy of transplanted islets, such as immunoisolation of islets by encapsulating semipermeable barriers, microencapsulation of individual islets by hydrogels,^{1–3} macroencapsulation of large number of islets by membranes,^{4–8} and hollow fibers containing alginate-encapsulated cells.^{9,10} Immunoisolating membranes must be biocompatible, biostable, nonfouling, implantable/explantable, flexible, highly O₂ permeable, sterilizable, soft, and smooth. At the same time, they must be semipermeable with precisely controlled nanometer sized conduits to allow rapid countercurrent in-diffusion of hydrophobic O₂ and hydrophilic species (water, metabolites, nutrients) and out-diffusion of insulin and wastes (CO₂), while excluding immune cells and large immunoproteins, such as immunoglobulin G (IgG, $M_n \sim 150\,000$ g/mol).

In the course of ongoing studies concerning membranes suitable for encapsulation/immunoisolation of living tissue, specifically pancreatic islets, a series of amphiphilic conetworks (APCNs) were designed in our laboratory.^{11–13} This new family of materials contain hydrophilic poly(dimethylacrylamide) (PDMAA) domains and hydrophobic polydimethylsiloxane (PDMS) domains cross-linked by grafts carrying PDMS branches fitted with vinylsilyl termini which upon cross-linking gave APCNs. These APCNs were specifically designed to contain cocontinuous hydrophilic and hydrophobic domains to allow the simultaneous and countercurrent diffusion of water (aqueous solutions) and oxygen.

Several research groups are currently engaged in the study of cocontinuous systems for diverse applications. Tiller and co-workers synthesized and actively used APCNs of diverse compositions for a wide range of different applications. These application have ranged from antimicrobial coatings¹⁴ to protection of enzymes¹⁵ and, more recently, enzyme entrapment and biocatalysis in organic solvents.¹⁶ Iván (who originally coined the term “amphiphilic conetworks”) and

Received: June 20, 2015

Revised: August 12, 2015

Table 1. Conditions for the Preparation of MA-PDMS-V Macromonomer^a

	MA-PDMS-V-0	MA-PDMS-V-1	MA-PDMS-V-2	MA-PDMS-V-5
V-PDMS-V(L) (17 200 g/mol)	0.250 mmol (100%)	0.248 mmol (99%)	0.245 mmol (98%)	0.238 mmol (95%)
V-PDMS-V(H) (117 000 g/mol)		2.5×10^{-3} mmol (1%)	5.0×10^{-3} mmol (2%)	12.5×10^{-3} mmol (5%)

^aEach composition contained SiHMA = 0.25 mmol, Karstedt's catalyst (3% xylene solution) = 0.02 mL, and toluene = 23 mL.

collaborators have worked for many years in the synthesis of a wide range different amphiphilic conetwork systems, providing also important insights into structural characteristics of conetworks.^{17–21}

Recent advancements include thermally responsive APCN systems²² and light responsive amphiphilic conetworks functionalized spiropyran and spirooxazine derivatives.²³ Tew's team proposed an ultraviolet-light-initiated thiol–ene end-linking platform that allows the conservation of cocontinuity within big variations in temperature, degree of polymerization, interaction strengths, and processing conditions.²⁴ In a recent publication, Chunju He et al.²⁵ synthesized conetworks of PDMS and PDMAA by end-cross-linking of amphiphilic triblock copolymers via atom transfer radical polymerization (ATRP). This conetworks showed promising properties for immunoisolation.

In earlier publications, we described the synthesis and swelling behavior,¹¹ biostability and biocompatibility,²⁶ and permeability and mechanical properties of APCN membranes.¹² Later, we described the synthesis of a semipermeable version of these immunoprotective APCN membranes.²⁷

Although the device exhibited fast insulin and bovine serum albumin (BSA) transport as well as low IgG diffusion via optimizing the dimensions of diffusion channels (by adjusting the molecular weight between cross-links, M_c) and met the above-mentioned criteria, it kept the islets alive for only 4 days in mice and 3 weeks in a dog. These results raised concerns in regard to the mechanical strength and channel dimensions of membranes. We theorized that the addition of controlled amounts of high molecular weight PDMS could remedy these problems. First, we attempted blending high molecular weight PDMS; however, the results were mixed with respect to mechanical stability. Our latest APCNs were prepared by the use of high molecular weight terminally functionalized PDMS to covalently attach this moiety to the rest of the network and thus to obtain a bimodal construct. Bimodal PDMS networks are excellent elastomers, exhibiting high ultimate strength and elongation.²⁸ The short chains convey ultimate strength and the long chains maximum extensibility.

The first section of this study presents a strategy for the synthesis of a new generation of bimodal amphiphilic grafts consisting of poly(*N,N*-dimethylacrylamide) (PDMAAm) main chain carrying two different molecular weight polydimethylsiloxane (PDMS) branches fitted with vinylsilyl and/or methacryl termini whose cross-linking leads to the target bimodal amphiphilic conetworks (bAPCNs). This approach was expected to increase the strength of membranes and to maintain controlled domain dimensions.

The second section concerns the effect of cross-linker ratio and amount of high molecular weight PDMS on membrane morphology, swelling characteristics, and mechanical properties in the swollen state.

2. EXPERIMENTAL SECTION

2.1. Materials.

Low molecular weight vinyl-ditelechelic PDMS (V-PDMS-V(L): molecular weight = 17 200 g/mol) and high molecular

weight vinyl-ditelechelic PDMS (V-PDMS-V(H): molecular weight = 117 000 g/mol), tetramethyldisiloxane, polyhydrosiloxane–PDMS copolymer (PHMS-*co*-PDMS) containing 30% PHMS, and Karstedt's catalyst (3% Pt in xylene, low color) were from Gelest. *N,N*'-Dimethylacrylamide (DMAAm), azobis(isobutyronitrile) (AIBN), allyl methacrylate, triphenylphosphine (PPh₃), tetrahydrofuran (THF), and toluene were supplied by Sigma-Aldrich.

For permeability testing, insulin from bovine pancreas powder, IgG from human serum ($\geq 95\%$), octyl β -D-glucopyranoside ($\geq 98\%$), and sodium azide ($\geq 99.5\%$) were supplied by Sigma-Aldrich. Insulin and IgG enzyme-linked immunoabsorbent assay (ELISA) kits were from ICL Lab.

2.2. Syntheses. **2.2.1. Synthesis of Asymmetric-Telechelic Macromonomer (MA-PDMS-V).** A previous publication¹¹ described the synthesis of 2-propionic acid-3-(1,1,3,3-tetramethyldisiloxanyl)-propyl ester (SiHMA). After synthesis, the components of charge were not separated, and the solution of the product mixture was used as is for the preparation of the grafts. Figure 2 shows the NMR spectrum of the product. V-PDMS-V(L) and SiHMA were placed in a 500 mL round-bottom flask and dissolved in freshly distilled toluene at room temperature. Then various compositions (1–5%) of V-PDMS-V(H) and V-PDMS-V(L) were added. Table 1 shows reagent quantities and stoichiometry. Hydrosilylation started by the addition of Karstedt's catalysts, and the charge was stirred 2 h while heating at 50 °C.

2.2.2. Synthesis of [PDMAAm(PDMS)]-g-PDMS-V (bAPG). Freshly distilled DMAAm (3.57 g), mixtures of low and high molecular weight MA-PDMS-Vs (0, 1, 2 and 5%, total 0.25 mmol), and 65 mL of toluene were placed in a 500 mL round-bottom flask under a nitrogen atmosphere. Then AIBN (5.36 mg) was added, and the system was stirred 24 h at 65 °C. The solvent was evaporated under vacuum, and the solid bAPG was recovered. Conversion was calculated as 95%. Depending on overall composition, i.e., on the amount of low and high molecular weight MA-PDMS-V, the products were optically clear rigid (MA-PDMS-V-0 and MA-PDMS-V-1) or flexible (MA-PDMS-V-2 and MA-PDMS-V-5) materials.

In order to calculate the molecular weight between cross-links (M_c), a homopolymer of DMAAm was also synthesized by using the conditions given above.

2.2.3. Cross-Linking BAPG to BAPCN and Membrane Preparation. A series of membranes were prepared as follows: bAPGs ([PDMAAm (PDMS)]-g-PDMS-V of 0, 1, 2, and 5%) (0.9 g) were mixed with the above cross-linker in three mole ratios (allyl chain end/hydrosiloxane = 1:5, 1:10, and 1:25) and cross-linked with a Karstedt's catalyst (25 μ L) in THF (8 mL). The bAPGs were homogenized with PHMS-*co*-PDMS cross-linker by strong stirring in THF for 10 min under a nitrogen atmosphere. Then the homogeneous solution was poured onto a Teflon surface and films of controlled thicknesses were prepared using a doctor's blade. Films were kept at room temperature overnight and cured 24 h at 70 °C. All bAPCN films were homogeneous and optically clear.

The nomenclature used for bAPCNs is XbAPCN1:Y, where X and Y represent percent V-PDMS-V(H) and moles of cross-linker, respectively.

2.3. Instrumentation and Instrumental Techniques. **2.3.1. Chemical Characterization.** ¹H NMR spectra were acquired on a Varian NMRS 500-MHz spectrometer by use of CDCl₃.

GPC traces were obtained with a Waters instrument equipped with Styragel columns (HR 0.5, HR 1, HR 3, HR 4, HR 5, and HR 6) and a refractive index detector (Optilab, Wyatt Technology). Samples were dissolved in THF, and the flow rate was 1 mL THF/min. Molecular weights were calculated using polystyrene calibration standards.

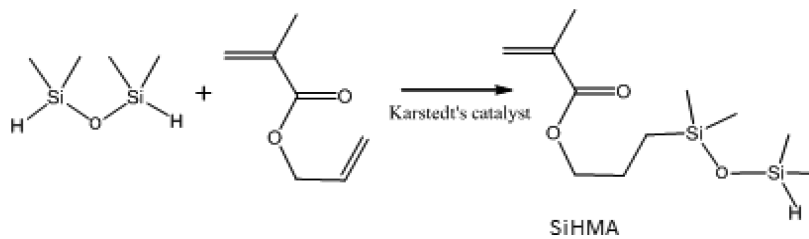


Figure 1. Synthesis of end-functionalizing agent (SiHMA).

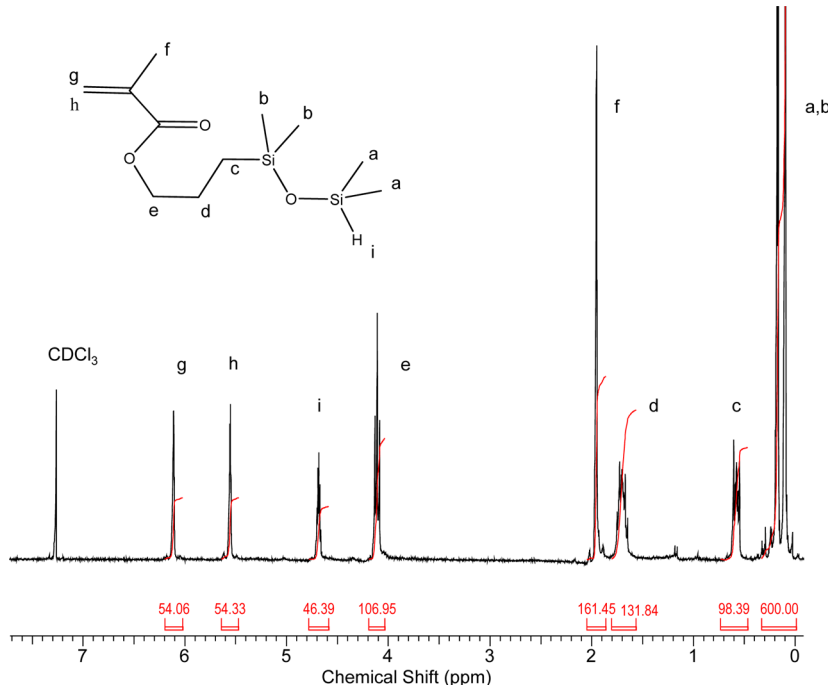


Figure 2. ¹H NMR spectrum of 2-propionic acid 3-(1,1,3,3-tetramethyldisiloxaniyl)propyl ester (SiHMA).

2.3.2. Structural Characterization. Gel permeation chromatography (GPC) elograms were obtained with a Waters GPC instrument equipped with a series of Waters Styragel columns (HR 0.5, HR 1, HR 3, HR 4, HR 5, and HR 6) and a refractive index detector (Optilab, Wyatt Technology). The samples were dissolved in THF, and a flow rate and column temperature were 1 mL of THF/min and 35 °C, respectively.

Gold-coated surfaces of APCN membranes were analyzed by an ESEM-FEG/EDAX Philips XL-30 (Philips, Eindhoven, The Netherlands) instrument using 10 kV accelerating voltage.

Solution-cast and cross-linked samples were examined by atomic force microscopy (AFM). The height and phase images were obtained using a Nanoscope III Multimode microscope from Digital Instruments operating in the tapping mode with aluminum-coated AFM probe (Nanosensors PPP-NCHR, length 125 nm, width 30 nm, thickness 4 nm, 330 kHz frequency).

Membrane surface compositions (top 10 nm) were determined by X-ray photoelectron spectroscopy (XPS), using a PHI VersaProbe II Scanning XPS Microprobe ultrahigh vacuum.

Films with high molecular weight PDMS content of 1, 2 and 5% and 1:5, 1:10, and 1:25 cross-linker ratio were tested.

2.3.3. Swelling Behavior. Swelling tests were performed with premeasured rectangular samples cut from bAPCN membranes (2 × 1 × 0.02 cm) and submerged in phosphate buffered saline (PBS) at room temperature. The extent of swelling was determined by periodically measuring the change in length with a traveling microscope. The swelling of bAPCNs was calculated by

$$V/V_0 = (L/L_0)^3 \times 100$$

where V , L and V_0 , L_0 are the volume, length of swollen and dry samples, respectively. Equilibrium swelling was recorded when swelling remained unchanged for 24 h at room temperature.

2.3.4. Permeability. Permeability tests were conducted by a diffusion chamber described earlier.¹² Thus, 60–90 μm thick membranes having a diffusion area of 2 cm² were placed between the receiver and donor chamber. The systems were mixed at 150 rpm at 37 °C to eliminate the boundary layer effect using a G24 Environmental Incubator Shaker from New Brunswick Scientific.

Insulin permeability tests were carried out using 400 μg/mL insulin (bovine, containing ~0.5% zinc) in PBS in the donor chamber. To prevent formation of insulin aggregates, solutions were stabilized with 0.15% *n*-octyl β-D-glucopyranoside, and 0.05% sodium azide antibacterial was added. Aliquots of 100 μL were taken every 5 min for the first 20 min. Insulin concentrations were determined by insulin ELISA, and a Spectramax Plus spectrophotometer was operated at 505 nm.

IgG permeability tests were carried out using 800 μg/mL human IgG in the donor chamber. For short time experiments, 100 μL aliquots were taken every 20 min for the first 60 min and for long time experiments the same amount every 12 h for 1.5 days. IgG concentrations were determined by human IgG ELISA using a Spectramax Plus spectrophotometer operated at 450 nm.

2.3.5. Mechanical Properties. A special bubble stretcher instrument developed in our laboratory coupled with a humidity chamber was used to study mechanical properties of APCN's under biaxial stretching. The instrument was designed and built specifically for testing of soft/swollen materials.²⁹ This instrument provides comprehensive and detailed characterization of mechanical behavior

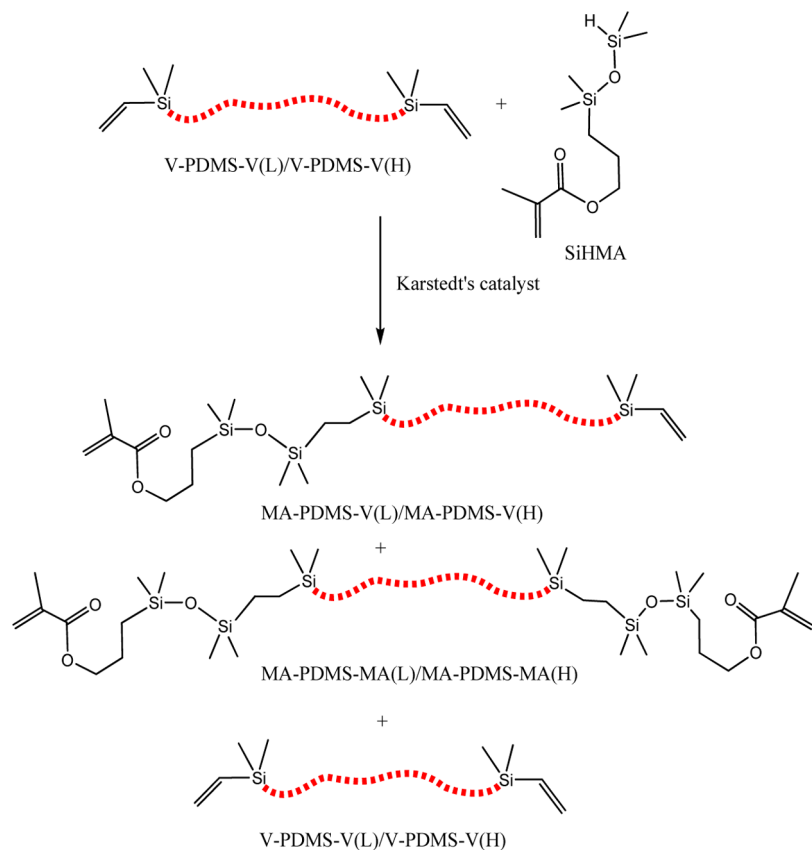


Figure 3. Hydrosilylation of V-PDMS-V by SiHMA. The dotted line stands for low or high molecular weight PDMSs.

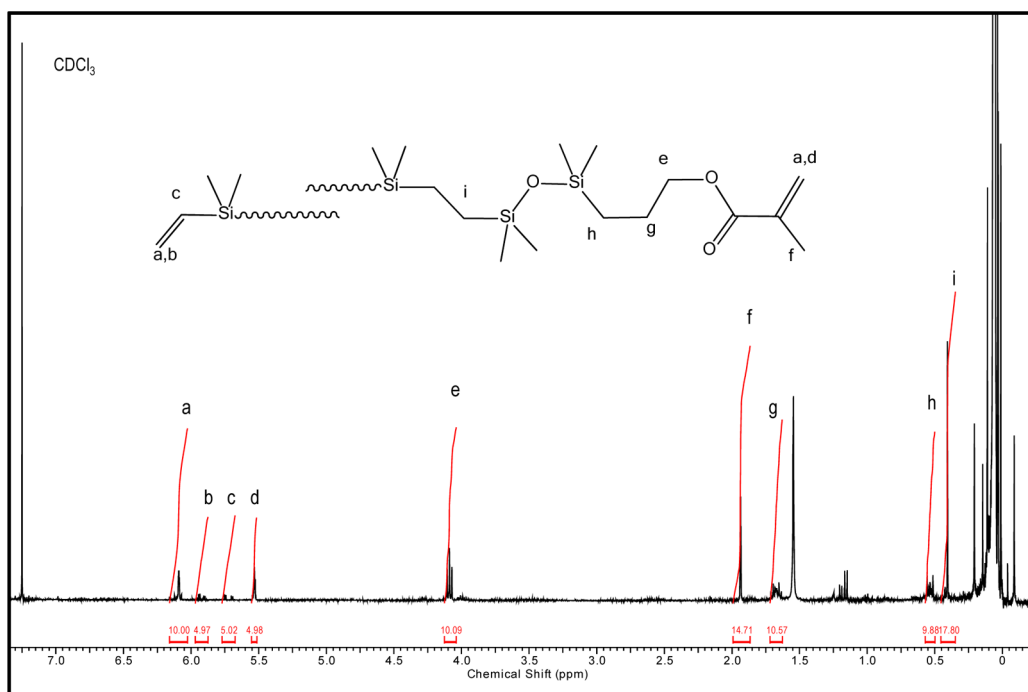


Figure 4. ^1H NMR spectrum of MA-PDMS-V.

of samples at a much greater detail than a regular tensile tester. Samples were gently clamped between two circular plates of 2.5 cm diameter aperture, which were in turn connected to a cylindrical chamber. Air was injected by a Harvard pump into the chamber, resulting in film deformation under gas pressure. Pressure change was recorded by a monitor while film deformation was determined by a

high speed camera. After analyzing pressure and deformation with ImageJ software, true stress and true strain were calculated. The device was placed in a humidity-controlled chamber in which the film swelled prior to testing. Samples with 1, 2, and 5% of V-PDMS-V(H) and 1:5, 1:10, and 1:25 cross-linker ratios were tested.

3. RESULTS AND DISCUSSION

3.1. Synthesis and Characterization. *3.1.1. End-Functionalizing Agent (SiHMA).* Figure 1 shows the synthesis of the end-functionalizing agent (SiHMA).¹¹ The function of SiHMA is to convert V-PDMS-V to the macromonomer MA-PDMS-V and the first cross-linker MA-PDMS-MA. The structure of SiHMA was confirmed by ¹H NMR spectroscopy (Figure 2). The spectrum shows a multiplet at 4.67 ppm due to the SiH group as well as characteristic resonances at 6.2 and 5.6 ppm due to olefinic protons and at 1.9 ppm for methyl protons associated with the methacrylate (MA) group.

3.1.2. Asymmetric-Telechelic Macromonomer (MA-PDMS-V). Figure 3 outlines the strategy for the synthesis of MA-PDMS-V. Thus, bimodal cross-linkable branches (MA-PDMS-V) of bAPG were prepared by combining SiHMA with two molecular weight (17 200 and 117 000 g/mol) vinyl ditelechelic PDMSs (V-PDMS-V(L) and V-PDMS-V(H))s by hydrosilylation. The reaction produces a statistical mixture of MA-PDMS-V(L)/MA-PDMS-V(H) (macromonomers), MA-PDMS-MA(L)/MA-PDMS-MA(H) (cross-linkable telechelic diacrylate), unreacted starting material V-PDMS-V(L), and V-PDMS-V(H). The product was characterized by ¹H NMR spectroscopy and GPC (Figures 4 and 5).

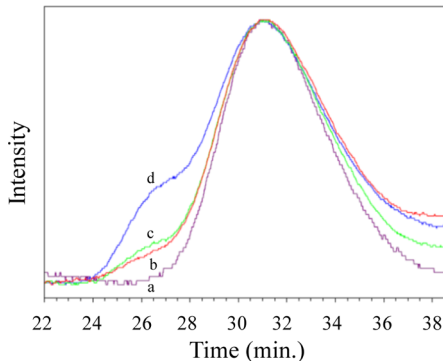


Figure 5. GPC traces of (a) MA-PDMS-V-0, (b) MA-PDMS-V-1, (c) MA-PDMS-V-2, and (d) MA-PDMS-V-5 (see Table 1 for abbreviations).

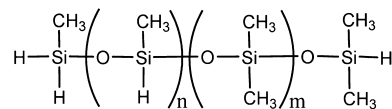
The ¹H NMR spectrum shows resonances characteristics of both MA and vinylsilyl groups. Resonances associated with SiH (4.67 ppm) are absent. The resonance for CH₂ due to hydrosilylation of Si-CH=CH₂ by SiHMA appears at 0.40 ppm.

The GPC traces in Figure 5 indicate that addition of MA-PDMS-V(H) could be followed with the shoulder appearing at high molecular weight region with increased intensities depending on composition. The M_n and polydispersities of MA-PDMS-V-0, MA-PDMS-V-1, MA-PDMS-V-2, and MA-PDMS-V-5 were found to be as 19 314 g mol⁻¹/1.50, 19 880 g mol⁻¹/1.77, 20 052 g mol⁻¹/1.87, and 22 167 g mol⁻¹/2.25, respectively.

3.1.3. Bimodal Amphiphilic Grafts (bAPG). The free radical terpolymerization of DMAAm plus MA-PDMS-V plus MA-PDMS-MA yields bAPG consisting of DMAAm backbone carrying -PDMS-V branches. As vinylsilyl termini do not copolymerize with DMAAm under free radical conditions,¹¹ the bAPG remains soluble. Figure 6 helps to visualize the synthetic strategy. Figure 7 shows that the position of the main elution peak of V-PDMS-MA shifts to higher number-average

molecular weights such as 29 646, 32 475, 33 273, 36 606 g mol⁻¹ with increasing V-PDMS-MA concentration, which indicates grafting. As expected, the polydispersity values exhibit a slight increase from 2.47 to 2.64 in a parallel manner.

3.1.4. Cross-Linking BAPG to bAPCN. The bimodal amphiphilic graft was cross-linked by hydrosilylation of -PDMS-V branches by polyhydrosiloxane-PDMS copolymer (PHMS-co-PDMS):



Crosslinker : PHMS-co-PDMS : 30 mol % PHMS

This copolymer inhibits shrinkage of membranes by supplying flexible PDMS spacers.

Figure 8 helps to visualize network formation by this cross-linker and the structure of the target bAPCN membrane. As bAPG, the cross-linker and the catalyst are soluble in THF, casting charges onto various surfaces (Teflon, glass, and stainless steel) produced colorless optically clear membranes.

3.2. Structural Characterization. Solution casting of polymers produces highly oriented skin layers during the early stages of drying.³⁰ As the film rests on a rigid substrate, its top layer expands resulting in anisotropic osmotic pressure,^{31–33} which in turn generates isotropic compressive stresses. The stress is applied on the top layer of the film that recedes over solvent-swollen softer compliant substrate. At a critical stress, the film buckles due to elastic instabilities.³² In the case of APCN, rapid evaporation of THF produces wrinkles with a regular pattern (see SEM images, Figure 9a). Crosby et al. showed that the characteristic wavelength of the wrinkle depends on the thickness and modulus of the skin:^{32–34}

$$\lambda = 2\pi h \left(\frac{\bar{E}_f}{3\bar{E}_s} \right)^{1/3} \quad (1)$$

where *h* is the thickness of the skin, *E_f* is the plane-strain modulus of the skin, and *E_s* is the modulus of the bulk (substrate). In order to establish quantitative mathematical correlations, the authors artificially controlled the skin layer formation to a known thickness.

The drying rate of a polymer–solvent system is controlled by several factors, including temperature, air speed, partial pressure of the solvent on the gas phase, polymer concentration, and the diffusion rate of the solvent through the polymer. Modifying temperature, solvent partial pressure, and/or air speed will significantly affect the kinetics of skin layer formation and development.³⁵ The multivariable complexity of the process makes the determination of the skin layer formation, its composition, and its transient thickness difficult on multi-component systems.

Figure 9a shows the decrease of wavelength of wrinkling instability from $\lambda = 2.5 \mu\text{m}$ (Figure 9a-I) to $\lambda = 1.25 \mu\text{m}$ (Figure 9a-II) with an increase in the amount of V-PDMS-V(H) at the same cross-linker ratio. These quantities were calculated by fast Fourier transform (see lower left corner of AFM images). The wavelength decreases to $\lambda = 0.8 \mu\text{m}$ with increasing cross-linker ratios (Figure 9a-III). According to eq 1, increasing skin layer modulus increases wrinkle wavelength. The modulus will depend on sample composition, which allows us to predict a lower Young's modulus of bAPCNs containing higher amounts V-PDMS-V(H).

Mixture of MA-PDMS-V(L)/MA-PDMS-V(H), MA-PDMS-MA(L)/
MA-PDMS-MA(H) and V-PDMS-V(L)/V-PDMS-V(H)

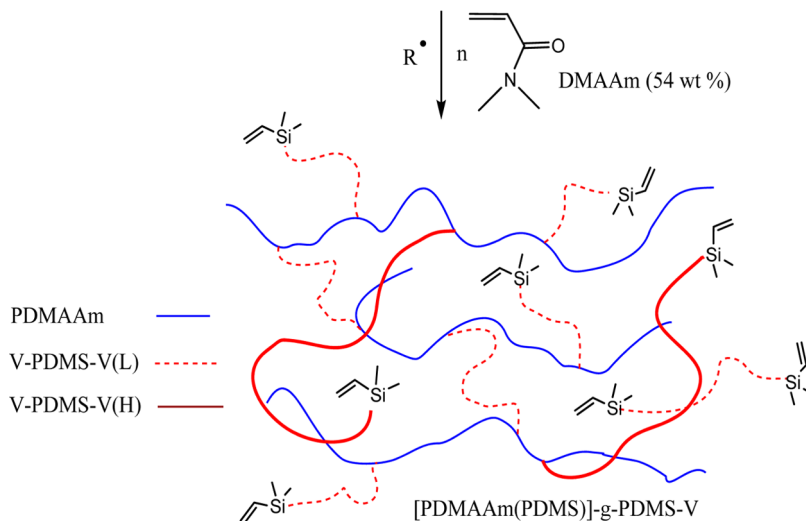


Figure 6. Strategy for the preparation of [PDMAAm(PDMS)]-g-PDMS-V (bAPG).

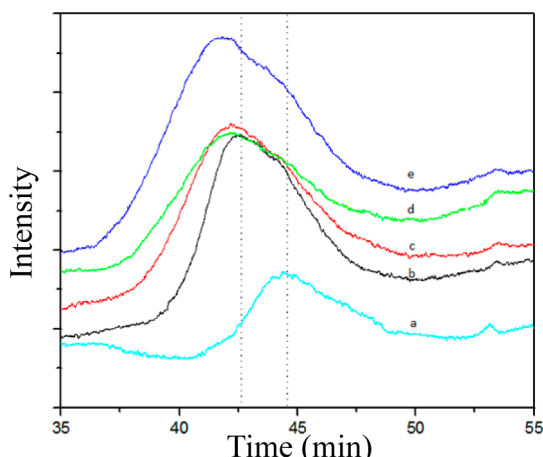


Figure 7. GPC traces of (a) V-PDMS-MA, (b) [PDMAAm(PDMS)]-g-PDMS-V-0, (c) [PDMAAm(PDMS)]-g-PDMS-V-1, (d) [PDMAAm(PDMS)]-g-PDMS-V-2, and (e) [PDMAAm(PDMS)]-g-PDMS-V-5.

Figure 9b shows AFM images of bAPCN films with 2 and 5% of V-PDMS-V(H) and 1:5, 1:10, and 1:25 allyl chain end/hydrosiloxane (cross-linker) molar ratios. The images show initial microphase separation, with the morphology and average domain size depending on bAPCN composition. This characteristic phase separation has been reported with other amphiphilic conetworks and was attributed to phase segregation due to random cross-linking.³⁴

Our hypothesis is quite different. We think the nanopattern is part of a multiscale diffusion-controlled wrinkling instability of the skin generated during film formation (Figure 9c). Kennedy et al.³⁶ showed that after film formation one of the components of the bAPCN tends to strongly concentrate on the surface due to minimizing surface energy. The nature of the component that comes to the surface depends on the medium the material is exposed. In dry-air it is the hydrophobic moiety that migrates to the surface due to its lower interfacial energy.³⁶ Thus, we propose that the domains observed on bAPCNs

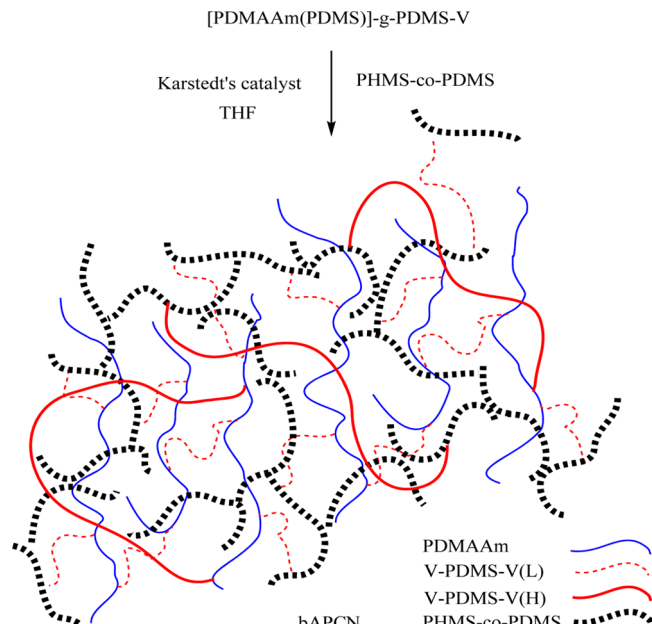


Figure 8. Schematic representation of formation of bAPCN.

surfaces are PDMS. XPS data substantiate this conjecture as it shows that the surface (top 10 nm) of all bAPCN grades is solely PDMS (Figure 9d). Peaks indicating carbon (Si-C at 283.5 eV), oxygen (siloxane at 531.14 eV), and silicon (siloxane at 101 eV Si 2p and 152.2 eV Si 2s) confirm the presence of PDMS on the surface, while the nitrogen peak expected at ~400 eV of PDMAAm is absent.³⁷ There is no experimental evidence that would indicate the presence of both hydrophilic and hydrophobic polymers on the surface of this particular system of bAPCNs. Amphiphilic conetworks respond to changes in the medium by morphological isomerization,³⁸ so even though the initial surface is hydrophobic, the swollen material can rearrange while in aqueous media to provide diffusion of metabolites.

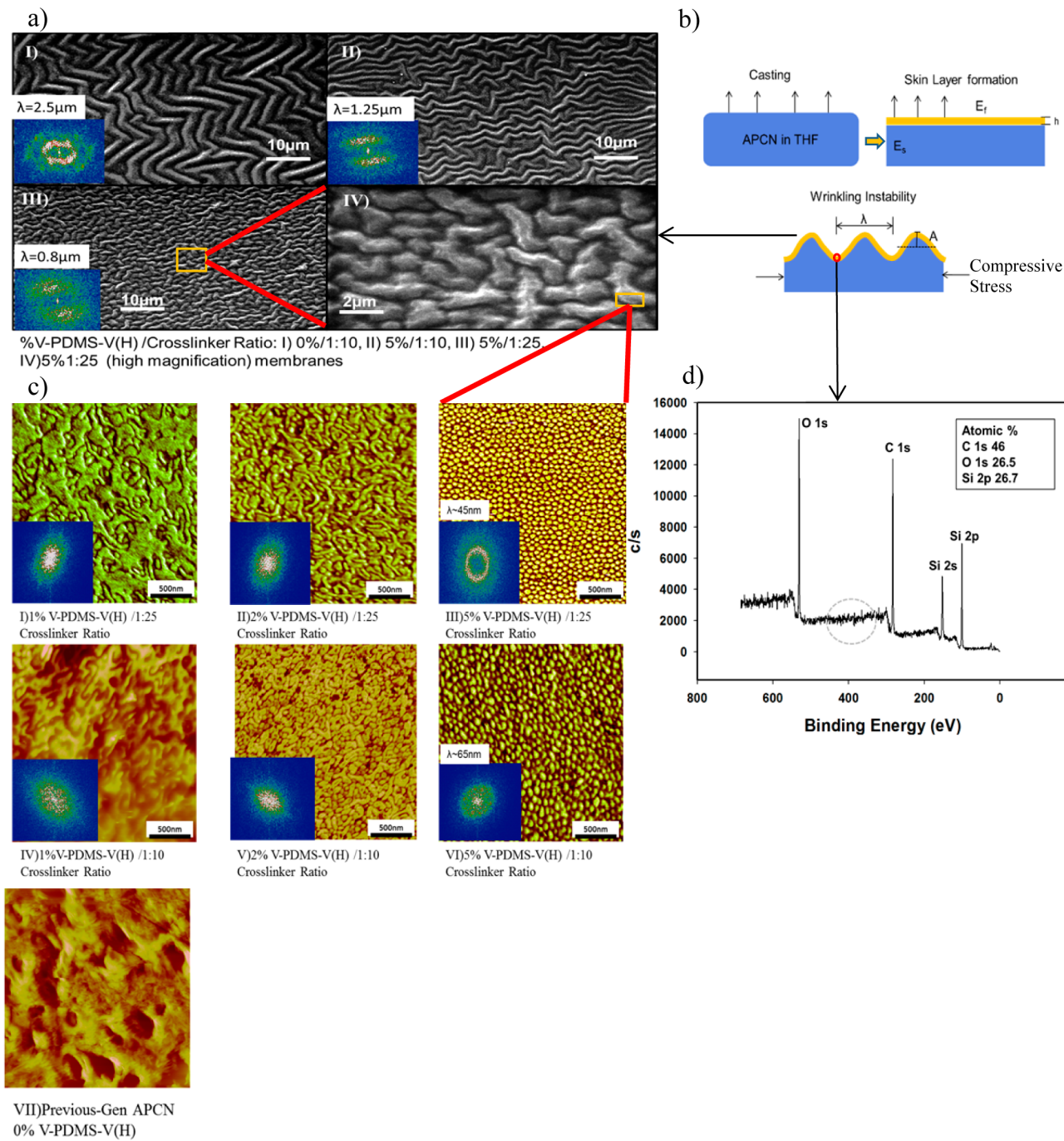


Figure 9. Multiscale, diffusion-controlled wrinkling instability morphology: (a) SEM images, (b) wrinkling instability model, (c) AFM images (height) of different APCN grades, including last generation, and (d) representative XPS data of the surface of the APCN.

In the absence of physical confinement, swelling/drying-induced wrinkles are isotropic and therefore exhibit randomly oriented broad size distributions.^{31,32} Thus, most bAPCN compositions do not exhibit long-range order with random domains, as indicated by AFM and fast Fourier transform images. The random powder spectrum in reciprocal space fails to show long-range domain size regularity. V-PDMS-V(H) concentration strongly reduces domain size (reduces the wavelength of wrinkling instability) and increases PDMS nanodomain regularity. In contrast, the degree of cross-linking had a lesser effect, it reduced only slightly domain size, and it had little to no effect on long-range order. This was anticipated as the copolymer-based cross-linker was expected to inhibit

shrinkage due to flexible PDMS spacers. Samples with 1% (at 1:10 (**Figure 9c-I**) and 1:25 (**Figure 9c-I**) cross-linker ratio) V-PDMS-V(H) show cocontinuous sponge-like morphology with large irregular domains. Conetworks with 2% (1:10 (**Figure 9c-V**) and 1:25 (**Figure 9c-II**)) cross-linker ratio) V-PDMS-V(H) exhibit elongated and significantly smaller asymmetrical PDMS domains. The bAPCN with the highest concentration of V-PDMS-V(H) (5%) and cross-linker ratio (1:10 (**Figure 9c-VI**) and particularly 1:25 (**Figure 9c-III**)) exhibits highly ordered monomodal homogeneous morphology with spherical domains. This is also seen in the fast Fourier transform image (**Figure 9c-III**), in which a single isotropic ring

in reciprocal space shows clear monomodal morphology, but with random spatial distribution.

Further evidence for drying-induced wrinkling instability was found by imaging a non-cross-linked sample over time. We theorized that the skin of a non-cross-linked sample would relax drying compressive stress and relax the wrinkling pattern. A sample containing 5% V-PDMS-V(H) and 1:25 cross-linker ratio was cast, dried, and sealed in a hermetic box, but not heated to avoid cross-linking. The sample was then imaged over several days. We observed an increase in the wavelength of the instability with time, as well as broadening size distribution, indicating relaxation of drying stress and wrinkling pattern. A fully cross-linked sample was also imaged as control, showing no distinct changes over time. The data can be found in the Supporting Information.

Surface topology and roughness are also important for immunoisolatory membranes. Smoother polymer surfaces are less thrombogenic.³⁹ Surface imperfections may trap microemboli and disrupt blood flow, resulting in thrombi. Equation 1 shows that the wavelength of wrinkling instability depends only on material properties and not on the level of compressive stress/strain that the film undergoes during drying. After the critical stress/strain necessary to initiate wrinkling instability is reached, extra stress/strain is accommodated by increasing the amplitude (A) of wrinkling while wavelength (λ) remains virtually unchanged:^{31–33}

$$A = h \sqrt{\frac{\varepsilon - \varepsilon_c}{\varepsilon_c}} \quad (2)$$

$$\varepsilon_c = \frac{1}{4} \left(\frac{3\bar{E}_s}{\bar{E}_f} \right)^{2/3} \quad (3)$$

where ε_c is the critical instability strain. Figure 10 shows the standard deviation of height profiles calculated after automatic baseline correction:⁴⁰

$$\sigma^2 = \frac{\sum_{i=1}^n (y_i - \langle y_i \rangle)^2}{n - 1} \quad (4)$$

where σ is the standard deviation of the corrected surface profile, n is the number of data points, y_i is the altitude at the i th surface position relative to the mean altitude, and $\langle y_i \rangle$ is the average of y 's.

It was observed that the surface topology of bAPCN is affected by both the concentration of V-PDMS-V(H) and cross-linker ratio. An increase in V-PDMS-V(H) content in bAPCN increased surface roughness. For samples with 1:25 cross-linker ratio, the change was particularly steep with the mean deviation in height increasing from ~15 Å at 1% V-PDMS-V(H) to ~52 Å at 5%. This effect was less significant for bAPCNs with a lower cross-linker ratio (1:10) with the mean deviation in height changing from ~23 Å at 1% V-PDMS-V(H) to ~35 Å at 5%. The cross-linker ratio had a similar tendency; i.e., higher cross-linker ratios suggest higher roughness.

Taking into account the difficulties in the determination of the transient thickness of the skin layer during film formation, all samples were prepared under the same drying conditions (concentration, temperature, solvent, and substrate type), making the total compressive stress experienced by the samples similar. This way, differences in roughness (i.e., wrinkling instability amplitude) correspond to differences in critical stress/strain that induces instability, i.e., composition-depend-

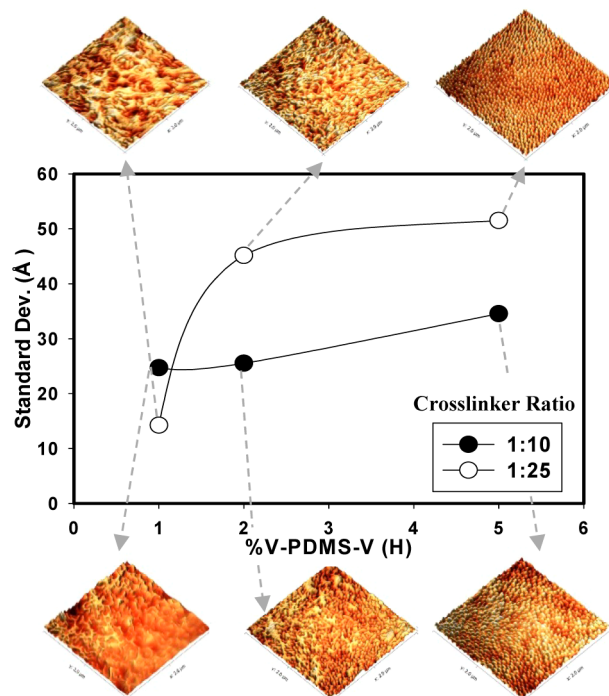


Figure 10. Roughness (amplitude) analyses for different bAPCNs grades.

ent moduli. Clearly, the elastic modulus of the skin (in eqs 1 and 3) decreases upon V-PDMS-V(H) addition, since wrinkling wavelength decreases and amplitude increases.³¹ A first approximation on the thickness of the skin layer will be provided after the mechanical characterization (see section 3.5).

Our ability to control both membrane domain spacing (λ) and roughness (A) through composition-dependent elastic wrinkling-instability may be important for biocompatibility.

3.3. Swelling. The swelling data in Figure 11 show that increasing cross-link density decreases swelling for all

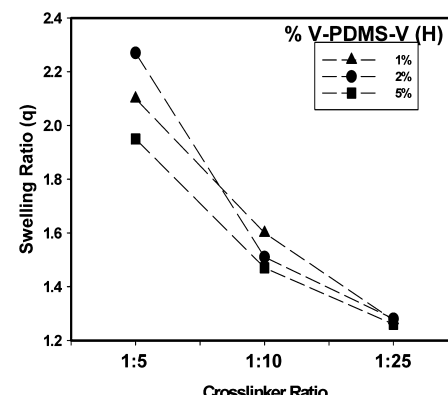


Figure 11. Swelling ratio of different bAPCN grades with varying % V-PDMS-V(H) and cross-linker ratio.

compositions. The increase in % V-PDMS-V(H) reduced the number of chain ends due to cross-linking, but this drawback can be neutralized by increasing the amount of cross-linker. Even though compositions with both high % V-PDMS-V(H) and cross-linker ratio were found to resist swelling in PBS, the obtained swelling level (~150%) is sufficient for efficient rates of diffusion of aqueous glucose and insulin.^{41,42} Importantly,

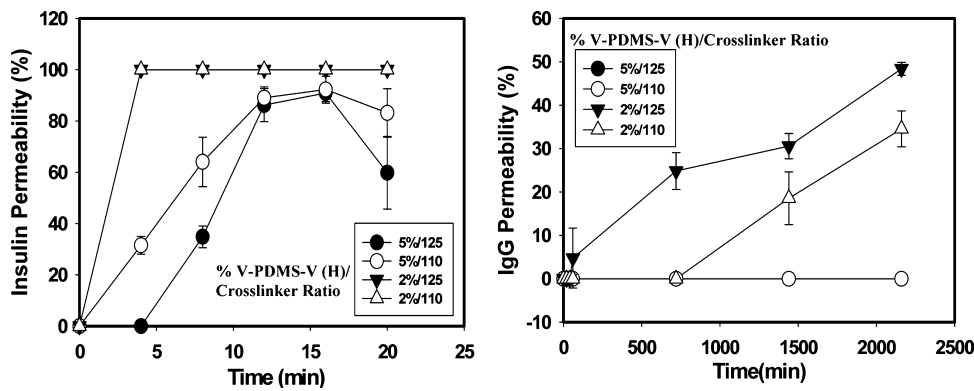


Figure 12. Permeability of insulin (left) and immunoglobulin G (right) vs time for different grades of bAPCNs varying % V-PDMS-V (H) and cross-linker ratio.

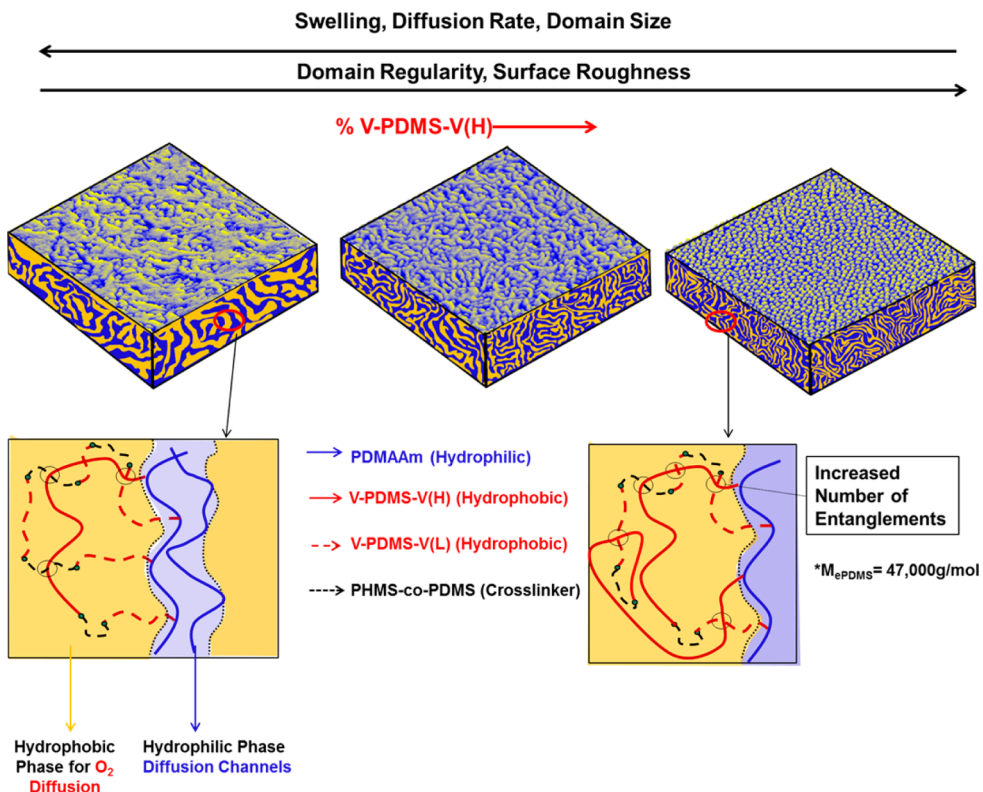


Figure 13. Amphiphilic conetwork: water-swollen PDMAA channels provide diffusion paths for insulin, and PDMS channels provide oxygen diffusion paths.

the high PDMS content (46%) of bAPCN makes this material a candidate for highly oxygen permeable immunoisolating membranes.

3.4. Permeability. Permeability studies of previous generations of APCN membranes focused on the effect of hydrophilic/hydrophobic ratios and molecular weight between cross-links of the hydrophilic component.¹² In the present work we focused on the effect of bimodality and cross-linker ratio of bAPCN membranes to block diffusion of IgG ($M_w = 150\,000\text{ g mol}^{-1}$) while allowing fast diffusion of insulin ($\sim 5700\text{ g mol}^{-1}$).²⁷

In the swollen state, both insulin and IgG permeate only through hydrophilic channels formed by water-swollen PDMAA domains. The dimensions of these channels are controlled by the molecular weight between cross-links (M_c) of

the hydrophilic moiety and by morphological thermodynamic/kinetic constraints on the network. M_c was calculated by

$$M_c = \frac{M_{n,\text{PDMAAm}} M_{n,\text{MA-PDMS-V}} W_{\text{PDMAAm}}}{(W_{\text{MA-PDMS-V}} M_{n,\text{PDMAAm}}) + (M_{n,\text{MA-PDMS-V}} W_{\text{PDMAAm}})} \quad (5)$$

where W_{PDMAAm} and $W_{\text{MA-PDMS-V}}$ are the weights of PDMAAm and acrylate end-functionalized PDMS, respectively, and $M_{n,\text{PDMAAm}}$ is the number-average molecular weight of PDMAAm determined by GPC, whereas $M_{n,\text{MA-PDMS-V}}$ is that of acrylate end-functionalized PDMS as calculated from ¹H NMR. With calculations based on experimental data, eq 5 yields $M_c = 9915\text{ g/mol}$.

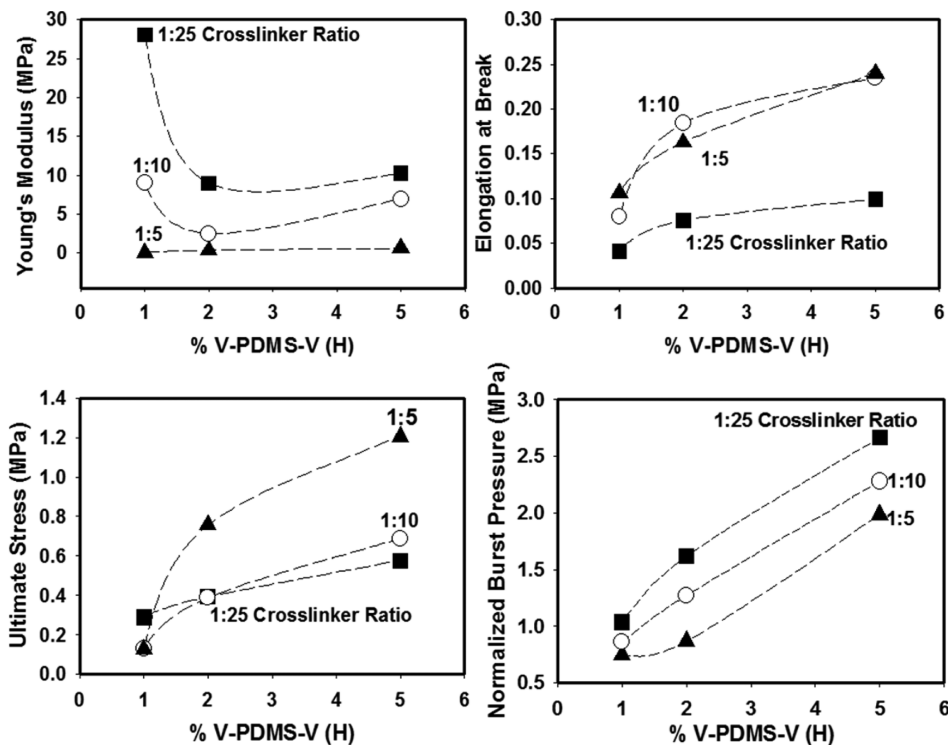


Figure 14. Calculated mechanical properties for swollen bAPCN grades under biaxial stretching.

Figure 12 shows the results of diffusion of insulin and IgG through different bAPCNs. Swollen bAPCN with low (1%) V-PDMS-V(H) content is not shown, as the membrane was too weak to withstand the extended diffusion. Higher cross-linker ratios contract the network and, as anticipated, reduce the diffusion rates of both insulin and IgG. Significantly, a high content of long-PDMS chains in the graft strongly reduces the diffusion rate of insulin and completely blocks the passage of IgG. With 2% V-PDMS-V(H), 25% of the IgG was able to penetrate the membrane in 36 h, while with 5% V-PDMS-V(H) IgG diffusion was completely blocked. Even though solutions were stabilized with *n*-octyl β-D-glucopyranoside, the insulin permeated concentration dropped after 16 h due to the insulin aggregation tendencies. As previously reported,¹² when insulin is exposed to hydrophobic surfaces (such as the walls of the chamber), it aggregates and adsorbs onto them, lowering its concentration in the solution.

We hypothesize that the presence of higher molecular weight PDMS increases the number of entanglements, which in turn reduces swelling and permeability. It is important that the molecular weight of the short chains be below the entanglement molecular weight M_e of PDMS (47 000 g/mol) while that of the long chains be considerably above this value.

Figure 13 helps to visualize these matters.

Previous generations¹¹ of APCN membranes only partially blocked IgG diffusion, due in part to the similarity of molecule sizes, while maintaining rapid insulin diffusion; the present generation of membranes achieves both objectives on account of better morphology control and the bimodal nature of the networks.

3.5. Mechanical Properties. Our calculations of true stresses and true strains of biaxially stretched bAPCN films follow Luchsinger,⁴³ who simplified the approach first proposed by Schmidt.⁴⁴ Schmidt rapidly quenched thermoplastic samples and directly measured the thickness to calculate true stress.

Since we cannot use this procedure, we assumed that the bubble formed during film deformation under gas pressure is of axisymmetric spherical geometry and that bAPCN is incompressible. The thickness of the specimen at the pole of the sphere was estimated by optically measuring the height of the bubble.⁴³

$$t_p = t_0 \left(1 + \frac{h^2}{a^2}\right)^{-2} \quad (6)$$

True stresses and strains at the pole were calculated by

$$\sigma_x = \sigma_y = \frac{PR}{2t_p} = \frac{P(a^2 + h^2)^3}{2ht_0a^4} \quad (7)$$

$$\varepsilon_x = \varepsilon_y = -\frac{1}{2}\varepsilon_z = -\frac{1}{2}\ln\left(\frac{t_p}{t_0}\right) = \ln\left(1 + \frac{h^2}{a^2}\right) \quad (8)$$

where P is the pressure by the pressure monitor, a is the initial radius of the film, R is the radius of the bubble, t_p is the thickness of the film during stretching, t_0 is the initial thickness of the film, and h is the height change of pole (analyzed by ImageJ software).

Our previous work on mechanical properties of APCN membranes concerned the effect of the hydrophilic/hydrophobic ratio on ultimate strength,¹² modulus, and elongation at break. The present work focuses on bimodal PDMS networks and on the effect of the cross-linker on modulus and ultimate properties.

Mark et al. carried out extensive work on mechanical properties of bimodal PDMS networks.⁴⁵ They showed that bimodal chain distribution greatly improves ultimate properties of PDMS networks. Thus, networks consisting entirely of short chains were brittle with relatively high modulus, ultimate strength, and low extensibility. In contrast, networks composed

of only long chains exhibited high extensibility but low ultimate strength.⁴⁵ The energy required to break either network is low, and neither would be considered a tough elastomer.

Mark and co-workers found that bimodal networks can have both high ultimate strength and maximum extensibility (corresponding to high rupture energies), which rendered them unusually tough.⁴⁶ Specifically, bimodal networks containing mostly short chains (~95%) showed greatly improved toughness and impact resistance over those of monomodal networks.⁴⁵ Low concentrations (<5%) of long chains gave lesser improvement, while high concentrations (>5%) made the material more rubbery with high extensibility but low ultimate strength.⁴⁵ Since PDMS does not undergo stress-induced crystallization at room temperature,⁴⁷ improved mechanical performance of bimodal networks was explained by proposing that short chains mainly increase ultimate strength through limited extensibility, while the elasticity of long chains stops fracture initiation that would lead to failure.

Similarly to bimodal PDMS networks, bAPCNs also showed greatly improved elongation at break and ultimate strength with increasing amounts of long PDMS chains. As seen in Figure 14, we observed a 2-fold increase in elongation at break and almost 5-fold increase in ultimate strength upon increasing the V-PDMS-V(H) content from 1 to 5%. bAPCNs with higher degrees of cross-linking exhibit both lower elongation at break and ultimate strength. Lower elongations are expected at higher cross-linker ratios, and ultimate true stresses are lower as less-stretched samples have larger cross-section areas. Young's moduli decreased with increasing amounts of V-PDMS-V(H) due to the higher elasticity of longer chains. The observed modulus vs % V-PDMS-V(H) trend was predicted by the decreasing wavelength and increasing amplitude of the wrinkling-instability patterns.

As a first approximation to calculate the thickness of the skin at the onset of the wrinkling instability, we can use the value of modulus of the dry APCN for the skin and that of swollen uncross-linked material for the bulk. For the sample with 5% V-PDMS-V(H) and 1:25 cross-linker ratio the experimental values of the moduli ($E_s = 15.4$ MPa, $E_m = 0.59$ MPa) and the wavelength of the wrinkles (~0.8 μm) are used to estimate the thickness of the skin, from eq 1

$$\frac{\lambda}{2\pi} \left(\frac{\bar{E}_f}{3\bar{E}_s} \right)^3 = h, \quad h \sim 58 \text{ nm}$$

Normalized burst pressures account for differences in thickness (see eq 9) and suggest the maximum pressure membranes can withstand during implantation.

$$P = \frac{Pa}{t_0} \quad (9)$$

where P is the pressure by the pressure monitor, a is the initial radius of the thin film, and t_0 is the initial thickness. As shown in Figure 14, burst pressure increases with both % V-PDMS-V(H) and cross-linker ratio. Immunoisolatory membranes are meant to withstand changes in hydrostatic pressure without damaging sensitive encapsulated tissue. Thus, higher burst pressure is desirable for islet encapsulating membranes.

4. CONCLUSIONS

We synthesized new cross-linkable bimodal amphiphilic grafts (bAPGs) of hydrophilic PDMAAm backbones carrying low ($M_n \sim 17\,200$ g/mol) and high ($M_n \sim 170\,200$ g/mol)

molecular weight hydrophobic PDMS branches and cross-linked them to bimodal amphiphilic conetworks (bAPCNs). A multiscale, composition-dependent elastic wrinkling instability arose during film formation due to network bimodality. The instability was shown to control both domain spacing (λ) and surface roughness (A), which in turn control surface morphology, a unique previously unseen feature in amphiphilic conetworks. bAPCNs produce semipermeable membranes exhibiting rapid insulin diffusion and impermeability to IgG. The coexistence of low and high molecular weight PDSMs in bAPCNs (i.e., bimodality) greatly improves ultimate mechanical properties and burst pressure of water-swollen bAPCNs. The novel bAPCN membranes are promising candidates for *in vivo* immunoencapsulation and other medical applications.

■ ASSOCIATED CONTENT

S Supporting Information

The Supporting Information is available free of charge on the ACS Publications website at DOI: [10.1021/acs.macromol.Sb01343](https://doi.org/10.1021/acs.macromol.Sb01343).

Figure S1 (PDF)

■ AUTHOR INFORMATION

Corresponding Author

*E-mail cakmak1@uakron.edu; Tel 330-972-6928 (M.C.).

Notes

The authors declare no competing financial interest.

■ ACKNOWLEDGMENTS

Our research was made possible by Ohio Third Frontier funding Wright Center program under CMPMD.

■ REFERENCES

- Dufrane, D.; Goebbels, R. M.; Saliez, A.; Guiot, Y.; Gianello, P. *Transplantation* **2006**, *81*, 1345–1353.
- Schneider, S.; Feilen, P. J.; Brunnenmeier, F.; Minnemann, T.; Zimmermann, H.; Zimmermann, U.; Weber, M. *Diabetes* **2005**, *54*, 687–693.
- Duvivier-Kali, V. F.; Omer, A.; Lopez-Avalos, M. D.; O'Neil, J.; Weir, G. *Am. J. Transplant.* **2004**, *4*, 1991–2000.
- Jesser, C.; Kessler, L.; Lambert, A.; Belcourt, A.; Pinget, M. *Artif. Organs* **1996**, *20*, 997–1007.
- Honiger, J.; Darguy, S.; Reach, G. *Int. J. Artif. Organs* **1994**, *17*, 46–52.
- Leoni, L.; Deasi, T. A. *Adv. Drug Delivery Rev.* **2004**, *56*, 211–229.
- La Flamme, K. A.; Popat, K. C.; Leoni, L.; Markiewicz, E.; La Tempa, T.; Roman, B.; Grimes, C.; Desai, T. *Biomaterials* **2007**, *28*, 2638–2645.
- Smith, C.; Kirk, R.; West, T.; Bratzel, M.; Cohen, M.; Martin, F.; Boiarski, A.; Rampersaud, A. *Diabetes Technol. Ther.* **2005**, *7*, 151–162.
- Altman, J. J. *J. Diabet. Complications* **1988**, *2*, 68–74.
- Trash, M. E., Jr. Master Thesis, Cleveland State University, 1997.
- Erdodi, G.; Kennedy, J. P. *J. Polym. Sci., Part A: Polym. Chem.* **2007**, *45*, 295–307.
- Kang, J.; Erdodi, G.; Kennedy, J. P. *J. Polym. Sci., Part A: Polym. Chem.* **2007**, *45*, 4276–4283.
- Erdodi, G.; Kang, J.; Yalcin, B.; Cakmak, M.; Rosenthal, K. S.; Grundfest-Broniatowski, S.; Kennedy, J. P. *Biomed. Microdevices* **2009**, *11*, 297–312.
- Tiller, J. C.; Sprich, C.; Hartmann, L. *J. Controlled Release* **2005**, *103* (2), 355–367.
- Bruns, N.; Tiller, J. C. *Nano Lett.* **2005**, *5* (1), 45–48.
- Dech, S.; Wruck, V.; Fik, C. P.; Tiller, J. C. *Polymer* **2012**, *53* (3), 701–707.

- (17) Iván, B.; Kennedy, J. P.; Mackey, P. W. *Polym. Prepr. (Am. Chem. Soc., Div. Polym. Chem.)* **1990**, 31 (2), 215–216.
- (18) Iván, B.; Kennedy, J. P.; Mackey, P. W. *ACS Symp. Ser.* **1991**, 469, 203–212.
- (19) Scherble, J.; Thomann, R.; Iván, B.; Mulhaupt, R. *J. Polym. Sci., Part B: Polym. Phys.* **2001**, 39 (12), 1429–1436.
- (20) Domjan, A.; Erdodi, G.; Wilhelm, M.; Neidhoefer, M.; Landfester, K.; Iván, B.; Spiess, H. W. *Macromolecules* **2003**, 36, 9107–9114.
- (21) Suevegh, K.; Domjan, A.; Vanko, G.; Iván, B.; Vertes, A. *Macromolecules* **1998**, 31 (22), 7770–7775.
- (22) Kali, G.; Vavra, S.; László, K.; Iván, B. *Macromolecules* **2013**, 46, 5337–5344.
- (23) Schöller, K.; Küpfer, S.; Baumann, L.; Hoyer, P. M.; de Courten, D.; Rossi, R. M.; Vetushka, A.; Wolf, M.; Bruns, N.; Scherer, L. *J. Adv. Funct. Mater.* **2014**, 24, 5194–5201.
- (24) Walker, C. N.; Bryson, K. C.; Hayward, R. C.; Tew, G. N. *ACS Nano* **2014**, 8, 12376–12385.
- (25) Xu, J.; Qiu, M.; He, C. *ACS Appl. Mater. Interfaces* **2014**, 6, 15283–15290.
- (26) Kang, J.; Erdodi, G.; Kennedy, J. P. *J. Polym. Sci., Part A: Polym. Chem.* **2008**, 46, 830–843.
- (27) Kang, J.; Erdodi, G.; Kennedy, J. P.; Chou, H.; Lu, L.; Grundfest-Broniatowski, S. *Macromol. Biosci.* **2010**, 10, 369–377.
- (28) Xu, P.; Mark, J. E. *Polymer* **1992**, 33, 1843–1848.
- (29) Guo, Y.; Drum, K.; Qu, C.; Cakmak, M. *Polym. Compos.* **2014**, 35, 4468.
- (30) Yucel, O.; Unsal, E.; Harvey, J.; Graham, M.; Jones, D. H.; Cakmak, M. *Polymer* **2014**, 55 (16), 4091–4101.
- (31) Chen, C. M.; Yang, S. *Polym. Int.* **2012**, 61, 1041–1047.
- (32) Chung, J. Y.; Nolte, A. J.; Stafford, C. M. *Adv. Mater.* **2009**, 21, 1358–1362.
- (33) Chung, J. Y.; Nolte, A. J.; Stafford, C. M. *Adv. Mater.* **2011**, 23, 349–368.
- (34) Bruns, N.; Scherble, J.; Hartmann, L.; Thomann, R.; Iván, B.; Mülhaupt, R.; Tiller, J. C. *Macromolecules* **2005**, 38 (6), 2431–2438.
- (35) Yucel, O.; Unsal, E.; Cakmak, M. *Macromolecules* **2013**, 46 (17), 7112–7117.
- (36) Kennedy, J. P.; Ratner, B. D. *Macromolecules* **1995**, 28 (8), 2595.
- (37) Louette, P.; Bodino, F.; Pireaux, J. *Surf. Sci. Spectra* **2005**, 12, 38.
- (38) Erdodi, G.; Kennedy, J. P. *Prog. Polym. Sci.* **2006**, 31 (1), 1–18.
- (39) Ikada, Y. *Adv. Polym. Sci.* **1984**, 57, 103–140.
- (40) Cakmak, M.; Simhambhatla, M. *Polym. Eng. Sci.* **1995**, 35 (19), 1562–1568.
- (41) Canal, T.; Peppas, N. A. *J. Biomed. Mater. Res.* **1989**, 23, 1183–1193.
- (42) Lustig, S. R.; Peppas, N. A. *J. Appl. Polym. Sci.* **1988**, 36, 735–747.
- (43) Galliot, C.; Luchsinger, R. H. *Polym. Test.* **2011**, 30, 356–361.
- (44) Schmidt, L. R.; Carley, J. F. *Polym. Eng. Sci.* **1975**, 15, 51–59.
- (45) Mark, J. E. *Macromol. Symp.* **2003**, 191, 121–130.
- (46) Xu, P.; Mark, J. E. *Polymer* **1992**, 33 (9), 1843–1848.
- (47) Xu, P.; Mark, J. E. *J. Polym. Sci., Part B: Polym. Phys.* **1991**, 29, 355–358.